# Solid Ink Printing with Dynamic Drop Size Modulation

*Steve Korol and Chris Greb*
*Office Printing Business Unit, Xerox Corporation*
*Wilsonville, Oregon*

## Abstract

While it is common that office solid ink printers utilize multiple drop sizes to produce different printing resolution modes, recently a system has been introduced implementing multiple drop sizes in a single printing mode. The advantage of this mode is in its higher image view quality at speed, which will be shown in some detail. Additionally, developmental particulars of this dynamic *drop size switching*, or DSS, print mode will be discussed. DSS printhead geometry will be presented together with an overview of the physics of multiple drop size ejection. With a system physically capable of DSS printing defined, a discussion of system implementation will follow. This discussion will include an analysis of the pertinent view quality and reliability requirements for the printing system. These requirements will be discussed as will the means found to meet them. Perhaps the most significant of these is the means by which jetting robustness goals were met through the use of a unique halftoning algorithm, which will be covered in detail. The paper will conclude with view quality comparisons of the solid ink DSS mode currently in the marketplace to a single drop mode of similar speed and another of similar view quality.

## Introduction

This research and development project is built on the efforts of the Xerox Office Printing Business Unit to develop a piezoelectric ink jet printhead capable of multiple drop size ejection. This printhead was first introduced in the Tektronix Phaser® 340 printer. It had two operational modes, one yielding a whopping 105 ng drop for the 300x300 DPI Standard mode, and a second delivering 65 ng for the 300x600 DPI Enhanced mode. While this printer and its siblings, the Phaser® 350 and 360, were capable of printing multiple drop sizes between prints, it was not until the recent introduction of the Phaser® 850 that such a printer had the capability to print multiple drop sizes within a print. (The Phaser® 850's DSS print mode uses a 51 ng large drop and a 24 ng small drop at 450x818 DPI.) It should be apparent to the reader that while switching drop sizes from print-to-print allows the user to select between optimal speed or optimal quality, dynamic drop size switching within a print allows a compromise in which higher apparent resolution may be realized without adversely impacting print speed. The benefit to the user of such a print mode is obvious.

As reported in earlier work, multiple drop sizes can be obtained from the same piezoelectric ink jet by appropriate waveform design.[1] Whether such multiple drop sizes are implemented in discrete printing modes or within one printing mode, the design principles are the same. This being said, the nature of the beast always seems to be that the details of the implementation make all the difference to the final product, and hence, to the customer. Indeed, while the DSS waveforms were developed irrespective of one another, the implementation of DSS in the Phaser® 850 forced them to be considered a pair, each influencing the behavior of the other.

In order to mitigate interaction of the two drop sizes, guidelines for their usage within a print were developed and a method for loosely enforcing the guidelines was devised. This means of enforcement is key to both the print quality of the DSS printing mode as well as its robustness. It is cast in terms of a halftoning algorithm and follows a background discussion of DSS jetting. In the final printer as in this paper, the DSS jetting fluidics and the DSS usage algorithm must be considered together in order to realize a product of any real quality.

## Jet Design, Jetting, and Drop Size Modulation

From a macroscopic viewpoint, the piezoelectric ink jet printhead of the Phaser® 850 is substantially similar to that of the Phaser® 340. Taking a closer look reveals differences in operating frequencies, number of jets, packing density, individual jet geometry, and drive waveforms. All of these parameters are related and must be balanced together to provide the best design. Figure 1 presents a cross-section of such a printhead. There are subtle geometric differences in every feature listed between the Phaser® 340 and 850. Needless to say, systems of such breadth lead to design schemes which are both complex and iterative. A calculated approach to jet design goes a long way toward limiting the number of logical permutations.

### Jet Design Overview

Breaking it down, the fundamental customer requirements of resolution, print speed (throughput), and robustness (reliability) provide a starting point. Once resolution requirements have been established, the number of

jets and firing frequency are determined. The possible combinations of these variables are bounded by the maximum possible jetting frequency and the required piezoelectric driver size to provide the largest necessary drop size.[2]

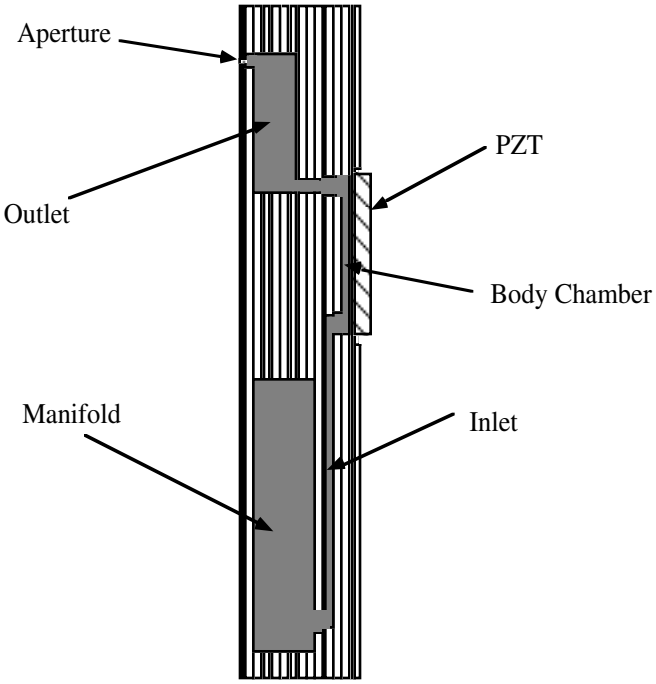


*Figure 1. Jet Stack Cross-Section*

Given operating frequency and number of jets, individual jet geometry can be determined. Higher operating frequencies require faster jets; faster jets generally require smaller features, and so on through the design. The intricacies of jet geometry are quite involved and beyond the scope of this paper. The interested reader may find more detail in the literature.[2] Suffice it to say that a compromise must be reached with manufacturing tolerances and jet-to-jet performance differences.

In concert with the fluid path, the piezoelectric driver (PZT) must be developed. Generally, driver design is a compromise between the size required to displace the largest drop desired and the high stiffness necessary for high natural frequencies. In both the Phaser® 340 and 850 printheads, an ink jet is fired by applying a drive voltage pulse (waveform) to a piece of PZT material that is attached to a thin diaphragm in contact with the ink-filled body chamber. The application of voltage to a PZT causes it to elongate or contract. Since one side of the PZT is constrained by the diaphragm, the resultant deflection is either concave or convex bending. This bending mode PZT driver was found to yield the best balance between electromechanical conversion efficiency, mechanical/fluid compliance, and manufacturability.[2]

**Waveform Design Overview**

Three fundamental modes are considered in ink jet waveform design: (1) the main, or Helmholz, mode, (2) the meniscus refill mode, and (3) the parasitic standing wave modes. The upper operating frequency (repetition rate) and drop ejection velocity of the main mode are driven by characteristics of the individual jet geometry and ink fluid. Namely, the inlet, outlet, and aperture inductances together with the outlet, mechanical, and fluid capacitances drive maximum drop frequency and velocity. Although not detailed in this paper, a lumped parameter model of an ink jet such as that in Figure 1, taking the above characteristics into consideration, is well known in the literature.[1,2] The upper operating frequency limit is known as the Helmholz frequency and is dictated by jet geometry. The Helmholz frequency yields a starting point for waveform development.

The estimate of upper operating frequency bounds the maximum length of the waveform. For example, an ink jet with a natural frequency of 40 kHz implies that the total length of the waveform should be around 25 µs in order to concentrate energy near the natural mechanical resonance of the device, thereby maximizing operating efficiency.

Given the length of the waveform, what of the shape? Figure 2 presents a plot of a waveform chain. The chain may be divided into two discrete waveforms and studied independently. The first waveform ends following the first low-to-zero rising transition and is characteristic of the 51 ng large drop of the Phaser® 850's DSS printing mode. The second zero-to-high rising transition begins the second waveform and is characteristic of the 24 ng small drop of the same mode.

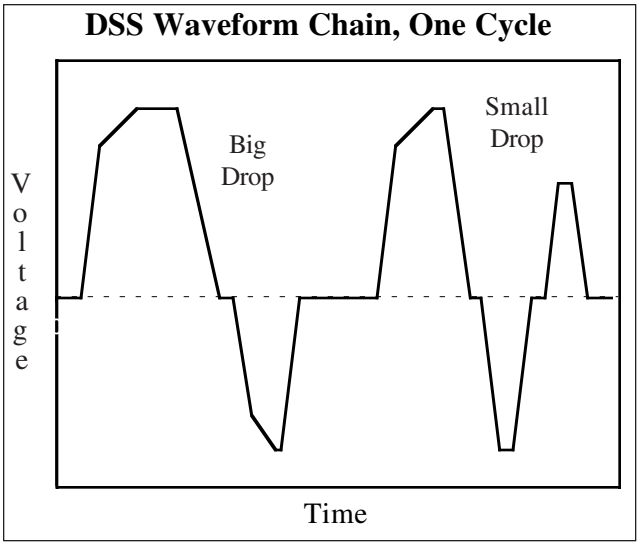


*Figure 2. DSS Waveform Chain*

For both waveforms within the chain, the shape and area under the curve prior to the first falling transition drives drop mass for a given jet. This first pulse dictates prefill of the jet. Drop ejection occurs during the high-to-low transition in the center of each waveform. Drop ejection

time may be measured and is generally in the neighborhood of one quarter of the total waveform duration.

Following drop ejection, the meniscus refills at a rate governed by the combined resistance of the jet inlet, outlet, and aperture, together with the meniscus capacitance. An equation for an estimate of this natural refill time is given in the literature.[1,2] As the natural refill time is slow compared to that of drop formation, the process is aided via the drive waveform. The negative pulse in each of the waveforms of Figure 2 serves to speed the refill rate.

Finally, the shape of the waveform may be tailored to aid jetting robustness and drop integrity. Parasitic standing waves within the inlet and outlet channels can yield resonances that decrease jetting efficiency and reliability. While one solution lies in adjusting jet geometry, this is often not possible due to jet packing issues within the printhead and manufacturing tolerances of the printhead. Therefore, the shape of the waveform may be further tailored to reduce energy near unwanted resonant mode frequencies. Additionally, fine tuning of the waveform allows such subtle changes as to affect the drop tail separation point and the mitigation of satellite droplets.

**Drop Size Modulation Overview**

Mathematical models suggest that several vibrational modes may be excited at the meniscus. Specifically, modeling the meniscus as a vibrating circular membrane leads to solutions described by Bessel functions of the first kind.[1,2] The higher the order of excitation, the narrower the zeroth order peak of the solution. When a forward moving flow is induced at this narrowed peak, smaller drops may be ejected.

The key to drop size modulation lies in the ink jet designer's ability to produce this forward moving flow over a reduced portion of the aperture. Success requires an understanding of drive pressure, internal flow, and meniscus surface dynamics. While a detailed analysis may be found in the literature,[3] a qualitative perspective is given in Figure 3. The first, second, and third order modes are plotted. The first order mode is also known as the bulk mode. The bulk mode, displacing the largest mass of fluid, yields the largest drop mass.

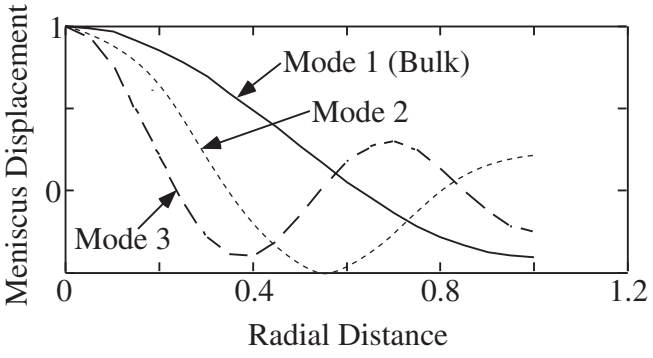


*Figure 3. Surface Wave Mode Shapes*

The large drop waveform presented in Figure 2 yields a bulk mode mass of 51 ng from the Phaser® 850 printer. The third mode, displacing the smallest mass of fluid of those plotted, yields the smallest drop mass. The small drop waveform presented in Figure 2 yields a third mode mass of 24 ng from the Phaser® 850 printer. Note the differences in the waveforms presented in Figure 2. As one would expect, the initial prefill pulse is larger for the big drop than for the small. Note further, though, the additional pulse following the negative refill pulse of the small drop waveform. This additional pulse serves to concentrate energy near the natural frequency of the surface mode desired (mode 3) and remove energy from the natural frequencies of competing modes. Energy near a harmonic of the main mode provides efficient higher mode operation. Efficiency may be further increased by boosting energy below the main mode natural frequency to aid refill rate.

Figure 4 presents stroboscopic digital micrographs of drops being ejected from the ink jet described above. The same jet was used to generate both drops, with the sole variable being waveform. The large drop on the left was generated with the bulk mode waveform; the small drop on the right was generated with the third mode waveform. Note especially the differences in meniscus size relative to drop size prior to drop ejection.

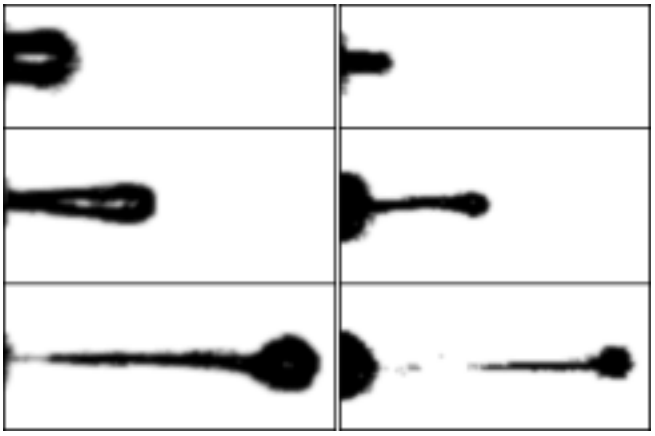

*Figure 4. Bulk and Mode 3 Drop Ejection*

## Dynamic Drop Size Modulation

It is no coincidence that within-print drop size modulation, or dynamic drop size modulation (DSS), was introduced some years following the first print-to-print drop size modulation capable printer. Aside from the fact that exciting a meniscus alternately in two entirely different ways presents an altogether new set of issues, implementation of such a print mode is substantially more complicated than that of a single drop size print mode. The complications ripple through the printer hardware and software: printhead drive electronics, printhead control firmware, printhead control software, image halftoning, and tone reproduction are just some of the pieces within a printer that are affected by the introduction of such a print mode. Of course, all of

these differences translate to increased cost to the customer and the question must be asked: will the benefit in print quality and speed more than offset this increased printer cost without adversely affecting reliability? Well, it took a few years to find the right answer.

**DSS Print Mode Driving Scheme**

The answer is a DSS printing mode that is a compromise between print quality and throughput, jetting reliability, and printer cost considerations. Interestingly, although not necessarily surprisingly, the latter consideration drove the former two. Given a DSS capable printhead, the focus turned to the methods by which to drive this new beast. A few options for drive electronics exist:

1. In the most straightforward implementation of DSS printing, the appropriate waveform (large drop, small drop, or no drop), would be generated on the fly for each jet and for every pixel of an image. Such an approach is simply not feasible, if not impossible, due to the vast hardware requirement to drive 448 jets in this manner.
2. In a second approach, similar to that of prior products, two separate waveform trains would be generated by the printer hardware, one for the large drop, and one for the small. The imaging algorithm would select one, the other, or neither, and the appropriate waveform would be directed to each jet for every pixel to be printed. This approach is essentially twice the drive hardware of previous products and was therefore deemed too costly.
3. A third approach would be to join the large and small waveforms together to form a chain as in Figure 2, consider each pixel two levels deep temporally, and select one waveform, the other, or neither from the chain for each jet and every pixel to be printed. This approach represents little or no hardware cost increase and minimal additional printer engineering effort.

Due to the cost, time, and engineering resource savings relative to the first two approaches, the third approach was chosen for productization. Of course, this approach hits a speed limitation much sooner than the prior two approaches, not to mention the robustness issues that may be brought about by exciting the meniscus not only by differing waveforms, but also at non-integral time intervals. Even so, initial laboratory experiments showed the benefits of DSS printing according to this scheme would be worth the potential risks.

**DSS Print Mode Halftoning Algorithm**

With the advent of multiple optical density inks and multiple drop deposition printing over the last few years, multilevel halftoning in desktop ink jet printers has become relatively commonplace. Even prior to these devices, multilevel halftoning schemes were not uncommon in monochrome laser printers. It was with such halftoning methods that the initial DSS prints were made. From these beginnings, several approaches were investigated prior to making the final halftoning approach decision. The final algorithm employed does not represent a radical departure from those common methods but is rather a carefully adjusted refinement. A discussion of these failed approaches as well as the final choice will aid the reader in understanding the intricacies of this DSS implementation.

All of the halftoning methods studied were based on blue noise, or high spatial frequency weighted noise, techniques. Of these, the first approach is very common indeed. This algorithm used either error diffusion methods with custom kernels operating on host-based raster image processors, or threshold array masks applied to the input image via an Adobe PostScript® interpreter. In both of these approaches the familiar binary case was simply extended to equal spacing of three levels. Greater detail on these methods is readily available in the literature.[4,5]

The trouble with such approaches was two-fold. The first issue is common to all such devices of relatively low spatial addressability and a couple of gray levels. False contours appeared in images halftoned according to these schemes due not to an insufficient number of gray levels, but rather due to differences in image granularity as a function of the tonal scale. This phenomenon will be described in greater detail within a few paragraphs.

While there are known methods of mitigating this texture induced false contour effect while maintaining the same basic halftoning scheme,[6] the second trouble with this approach rendered further work on this general class of algorithms futile. Namely, jetting robustness was found to be questionable for DSS printing of areas containing high frequency mixing of small and large drops. Analytical testing that followed determined certain large and small drop ejection combinations were to blame for the robustness issue. Although the root cause of the robustness issue was never determined, it is likely due to the specific print mode drive scheme. It is entirely possible that residual disturbances in the meniscus from the firing of certain previous drop sequences led to instabilities in subsequent firings. Whatever the explanation, given project schedule pressures, the only viable solution was to avoid these small and large drop combinations during printing.

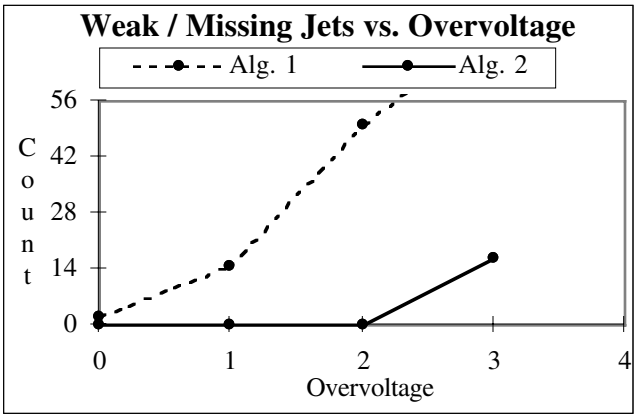


*Figure 5. Effect of Halftoning Algorithm on Robustness*

Figure 5 reveals experimental results in which two halftoning algorithms were tested for robustness. The response variable, the number of weak and/or missing jets

within a number of prints, was measured for nominal drive voltage and overvoltage stress testing. The difference between the two algorithms is in the combinations of small and large drops that are permitted to be printed. It is clear from this figure that it is possible to vastly improve jetting robustness by carefully tuning the halftone algorithm.

In order to meet the robustness criteria, it was clear that certain combinations of large and small drops had to be avoided. Taking these forbidden patterns into consideration and building on the previous experience with DSS halftoning, attempts were made to filter these patterns out of the image to be printed. The patterns were removed both by building threshold arrays that omitted them as well as post processing three-level bitmaps to eradicate them. In all attempts, however, although robustness was dramatically improved, as in the second curve of Figure 5, visible patterning was introduced into the halftoned image.

To illustrate this point, Figure 6 presents two density plots of the Power spectra for DSS prints at a given percent tint. The Power spectra were computed as in previous research on solid ink print quality[7] and are centered about 0, with limits of plus and minus 15 cycles/mm. The plot on the left was generated from a print made with the halftoning method of Figure 5 Alg.2, whereas the right-hand plot was generated from a print made with the hafltoning method of Figure 5 Alg. 1. The plots demonstrate the dramatic introduction of low frequency power into the halftoned image, transforming the blue noise halftoning scheme into much more of a white noise approach. Such objectionable print quality was deemed unacceptable regardless of the positive impact on robustness.

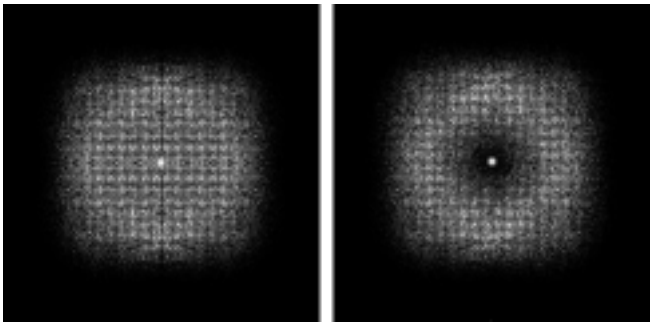

*Figure 6. Power Spectra Density Plots for Two DSS Prints*

At this point, it was known that there were two desired traits the successful DSS halftoning algorithm had to possess given the print mode driving scheme employed. Simply stated, it had to allow the usage of small and large drop sizes while (1) omitting certain firing combinations of the two drops and (2) maintaining blue noise characteristics. The key to defining an algorithm able to meet the above criteria was actually published prior to this work[7]. The nature of the offset solid ink printing process is such that physical dot gain spreads isolated printed dots to a much greater degree than constrained or even semi-constrained dots. Further, this physical dot gain causes the peak in granularity to shift well below the 50% digital coverage expected for systems with low dot gain. Combining these two facts points one squarely in the direction of the halftoning method finally employed. It takes advantage of the need to replace large dots with small only over about the first half of the input scale, a requirement that can be met while maintaining blue noise characteristics and only very infrequently printing the aforementioned forbidden drop patterns. It represents a compromise in which the full benefit of small drop printing is not realized and the robustness jet firing rules are not explicitly followed, but rather the frequency of their violation is limited.

Specifically, using a conventional blue noise halftone screen represented as a threshold array, the algorithm ramps through graylevels in the order dictated by the array, beginning first with small drops. The grid continues to be filled with small drops until a peak value is reached, beyond which point big drops replace small drops following the order in which the small drops were initially placed. Once all of the small drops have been replaced with large drops, large drops continue to fill the grid according to the blue noise halftone screen until no vacancies remain. Figure 7 illustrates the algorithm for a sample 4x4 blue noise cell with a peak value of 25%, where the numbers in the cells represent the placement order. Italicized numbers represent small drops and the remaining numbers represent large drops. After 25% of the array is addressed with small drops, big drops begin replacing the small drops preferentially until the entire grid is filled with large drops and a solid fill is achieved.

| | | | |
|---|---|---|---|
| 14 | *1* 5 | 18 | 11 |
| 8 | 15 | 10 | *3* 7 |
| 16 | 9 | 12 | 19 |
| *0* 4 | 17 | 13 | *2* 6 |

*Figure 7. DSS Halftone cell example*

Figure 8 represents the scheme by which a DSS halftone cell is filled according to the algorithm described above. The abscissa represents the input percent gray and the ordinate the output digital percent coverage. Note that depending on the input request, the output may be comprised of small drops, big drops, or a combination of the two. As plotted, small dots increase at a slope of m1 until the peak value (labeled Peak) is reached. At this point, large dots begin replacing the small dots until no small dots remain (labeled Max). Note that slopes m2 and m3 are inverses of one another. Beyond the input point corresponding to Max, all small dots have been replaced and large dots continue to fill the grid according to slope m4, which is chosen

according to gamma desires. Any adjustments made to tone reproduction must be made in such a way so that the parameters described above are not overridden. Adjustments such as these represent adjustments to the input request prior to algorithm implementation.

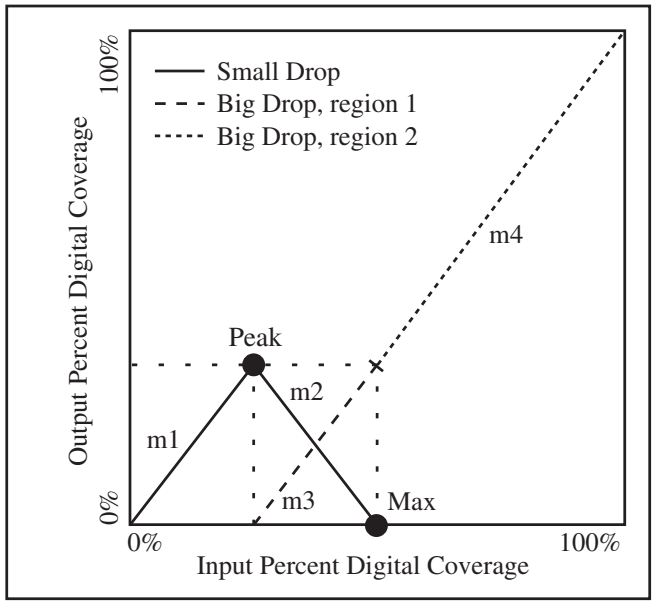


*Figure 8. DSS Halftoning drop usage graph, including critical setpoint and slope parameters*

## Application and Results

Two issues provide bounds for the critical parameters used in Figure 8. In general, image quality increases as the Peak moves toward the point (50,100). This would represent full utilization of the small drop. As mentioned earlier, however, due to the dot gain behavior of solid ink, a point of diminishing return is reached somewhere around 50% digital coverage of the small dot. In a sense, robustness moves in opposition to image quality in this implementation of DSS, so that the greater the usage of the small dot, the greater the robustness risk. For these reasons, the Peak and Max values were chosen to maximize image quality while balancing robustness risk.

Figure 9 presents a plot of granularity vs. reflectance for a few print modes. This measurement of image granularity is defined in the literature[8] as

$$g = \sqrt{\frac{\int_{-V}^{V}\int_{-U}^{U} W(u,v)VTF^2(u,v)dudv}{\int_{-V}^{V}\int_{-U}^{U} VTF^2(u,v)dudv}} \qquad (1)$$

where the VTF is the Visual Transfer Function, the eye's response to spatial frequency. The VTF at frequencies less than 1.0 cyc/mm is equal to one; and equal to equation (2) otherwise.

$$VTF(u,v) = 5.251e^{-0.7609\sqrt{u^2+v^2}}(1-e^{-0.5236\sqrt{u^2+v^2}}) \qquad (2)$$

Granularity as defined above is simply the Power spectrum of the image, *W(u,v)*, filtered by the VTF. It has been used as a metric for solid ink prints with good success in the past[7] and again seems to correlate well qualitatively with visual response. As can be deduced from the data presented, the higher the granularity index, the more grainy the print. The 51 ng print is by far the worst example for graininess. Note especially the degree to which DSS printing mitigates granularity. The curve labeled DSS T2 was generated through use of the final halftoning algorithm. It nearly matches the 600x1200 DPI, 24 ng high quality print mode over the entire tonal range. DSS T1 was generated via the conventional multi-level halftoning method initially employed. While the average print granularity is indeed lowest for this mode, the sharp valley between the granularity peaks led to the visually objectionable texture contouring mentioned earlier.

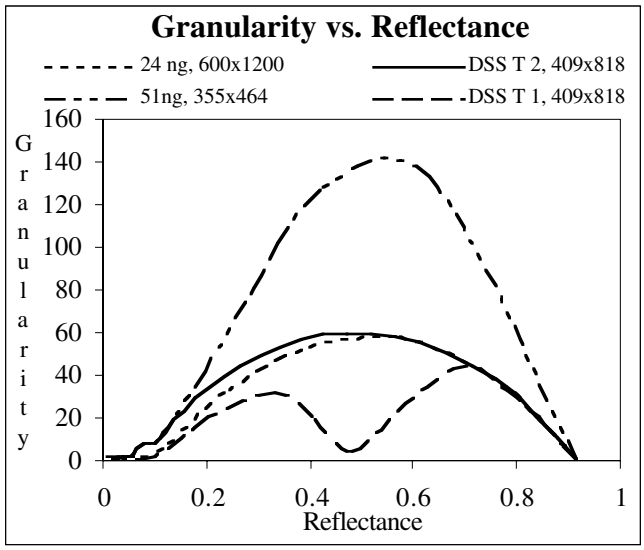


*Figure 9. Granularity vs. Reflectance for several print modes*

Figure 10 reveals digital micrographs of a few samples from the granularity curves of Figure 9. Note the high granularity of the 51 ng print in the upper left. The sample in the upper right was generated via the preferred DSS halftoning algorithm. Compared to the lower left image, corresponding to the 24 ng print, the granularity is about the same at normal viewing distance. The combination of large and small dots within this print is indicative of the print mode. In the lower right corner is a print at the valley minimum of the DSS T1 curve of Figure 9. This is a solid fill generated with small drops. It is because this uniform solid fill is decimated on either side that texture contouring occurs. Given the plot of Figure 9 together with the

micrographs of Figure 10, the print quality advantage of DSS printing is clear.

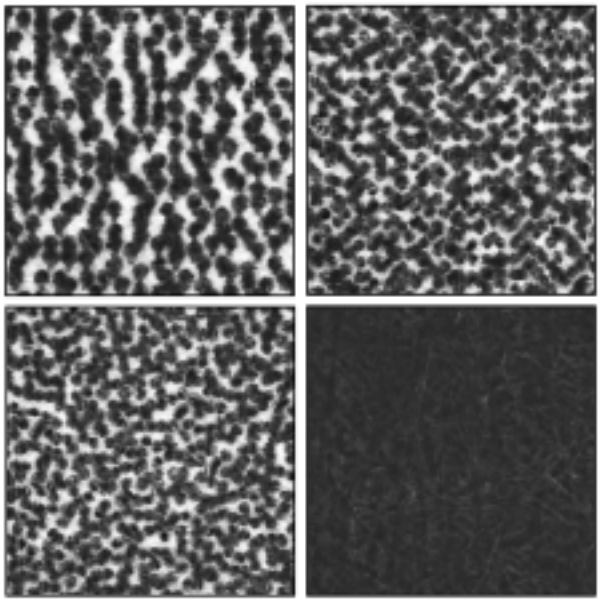

*Figure 10. Digital Micrographs of Granularity Samples*

## Conclusions

The Phaser® 850 provides a solid example of productized DSS printing. It builds on the strengths of its predecessors by not only containing print-to-print drop size modulation with its 51 ng 355x464 DPI and 24 ng 600x1200 DPI print modes, but also by introducing within-print dynamic drop size modulation, or DSS. The advantage of DSS printing is in it's high print quality at speed – print quality that rivals that of the printer's high resolution mode for photographs and graphics. It is, however, not without limitation. The penalty for the increased speed is the coarse grid relative to the high quality mode (450x818 DPI vs. 600x1200 DPI). Even so, for the majority of printing tasks, this mode will suffice. In fact, one anonymous representative of the Office Printing Business Unit's marketing department was heard saying "This [print] mode is too good. There is not enough differentiation between it and our Photo mode."

Future implementations of DSS will likely involve specifically tailored driver hardware to work in concert with a DSS capable printhead. Although such an approach adds hardware cost, the benefits of higher maximum operating frequencies and further print quality improvements together with reduced robustness risk may well outweigh the additional costs over the life of the product. Further, future implementations may take advantage multiple higher order meniscus vibrational modes in addition to the bulk mode. In such a product, four or more distinct drop sizes could well be realized.

## Acknowledgements

This paper summarizes some of the fluid, print quality, and systems design aspects of the Phaser® 340 and 850 solid ink printers, which were joint efforts of many employees at the Office Printing Business Unit of the Xerox Corporation.

A special debt of gratitude is owed to Ron Burr for his effort not only as an extraordinary fluid physicist, but also as the motivating force behind this implementation of DSS printing.

## References

1. R.F. Burr, D.A. Tence, and S. Berger, Multiple Dot Size Fluidics for Phase Change Piezoelectric Ink Jets, *Proc. NIP12*, pg. 12. (1996).
2. R.F. Burr, S. Berger, and D.A. Tence, Overview of Phase Change Piezoelectric Ink Jet Fluids Modeling and Design, *Proc. of the ASME*, **239**, pg. 545. (1996).
3. R.F. Burr, D.A. Tence, H.P. Lee, R.L. Adams, and J.C. Mutton, "Method and Apparatus for Producing Dot Size Modulated Ink Jet Printing", U.S. Patent 5,495,270, 1996.
4. R. Ulichney, **Digital Halftoning**, MIT Press, Cambridge, Massachusetts, 1996.
5. _____, **Adobe PostScript Language Reference Manual, Second Edition**, Addison-Wesley Publishing Company, New York, 1990.
6. Q. Yu and K.J. Parker, Digital Multitoning Evaluation with a Human Visual Model, *Proc. NIP13*, pg. 579. (1997).
7. S. Korol, The Effects of Ink and Media Parameters on Offset Solid Ink and Xerographic Halftoned Image View Quality, *Proc. PICs*, pg. 210. (1998).
8. M. McGuire, R. Shaw, Autocovariance Techniques for the Practical Evaluation of Digital Image Noise *Proc. NIP13*, pg. 566. (1997).